

**From nanosized precursors to high performance ceramics: The case of  $\text{Bi}_2\text{Ca}_2\text{Co}_{1.7}\text{O}_x$** 

M. A. Madre<sup>1,\*</sup>, Sh. Rasekh<sup>1</sup>, K. Touati<sup>2</sup>, C. Salvador<sup>1</sup>, M. Depriester<sup>2</sup>, M. A. Torres<sup>1</sup>, P. Bosque<sup>1</sup>, J. C. Diez<sup>1</sup>, A. Sotelo<sup>1</sup>

<sup>1</sup>Instituto de Ciencia de Materiales de Aragón (CSIC-Universidad de Zaragoza), M<sup>a</sup> de Luna, 3, 50018-Zaragoza, Spain.

<sup>2</sup>UDSMM (EA 4476), MREI-1, Université du Littoral Côte d'Opale, 59140 Dunkerque, France

**Abstract**

$\text{Bi}_2\text{Ca}_2\text{Co}_{1.7}\text{O}_x$  thermoelectric ceramics were prepared by four different synthesis routes: coprecipitation with ammonium carbonate or oxalic acid, attrition milling, and solid state (as reference). Microstructure showed that coprecipitation and attrition milling produced sintered materials with less porosity and smaller particle sizes than the solid state ones. Thermoelectric properties reflect the microstructure, leading to materials with lower electrical resistivity and higher Seebeck coefficient, when compared with the solid state ones. In spite of an increase in thermal conductivity in these samples due to their lower porosity, the maximum estimated Figure-of-Merit is higher than in sintered materials.

**Keywords:** Electroceramics; Sintering; Electrical properties; Microstructure.

\* Corresponding author: M. A. Madre. [amadre@unizar.es](mailto:amadre@unizar.es). Dept. Ciencia de Materiales; C/M<sup>a</sup> de Luna, 3; 50018-Zaragoza; Spain. Tel: +34 976762617.

## 1. Introduction

Thermoelectric (TE) conversion is an effective technology that allows directly transforming thermal to electrical energy. It is considered one promising method to raise the efficiency of classical energy transforming systems, reducing CO<sub>2</sub> emissions, and helping to fight against global warming. On the other hand, it is still necessary to raise the efficiency of these TE materials, quantified through the dimensionless Figure-of-Merit, ZT, defined as  $TS^2/\rho\kappa$ , where T, S,  $\rho$ , and  $\kappa$ , are the absolute temperature, Seebeck coefficient, electrical resistivity, and thermal conductivity, respectively [1]. Nowadays, semiconducting and intermetallic materials are used in TE modules with high performances, but many are composed by heavy and/or toxic elements (Sb, As) which can melt or oxidize at high temperatures. These factors and their low abundance in earth's crust, limit the number of possible applications. The discovery of high thermoelectric performances in Na<sub>x</sub>CoO<sub>2</sub> [2], composed of non toxic, cheap, abundant, and environmentally friendly elements, provided a solution. As a consequence, new oxide materials have been explored, leading to the discovery of other layered cobaltites [3-6]. Anyway, their TE properties must be increased before considering them for practical applications [7]. One strategy exploits their anisotropy to align their grains [8-10], decreasing  $\rho$ , while other tune up the thermoelectric parameters via doping [11,12]. On the other hand, only few works explore the synthesis methods, as usually samples are prepared by solid state [8,13], or sol-gel [9,14] routes.

In this work, four different synthesis methods (coprecipitation using ammonium carbonate or oxalic acid, attrition milling, and solid state) will be used to determine the effect of initial particle size and homogeneity on the microstructure and thermoelectric performances of Bi<sub>2</sub>Ca<sub>2</sub>Co<sub>1.7</sub>O<sub>x</sub> sintered materials.

## 2. Experimental

Bi<sub>2</sub>Ca<sub>2</sub>Co<sub>1.7</sub>O<sub>x</sub> ceramics produced by coprecipitation were prepared from Bi<sub>2</sub>O<sub>3</sub> (99.9%, Aldrich), CaCO<sub>3</sub> ( $\geq 99\%$ , Aldrich), and Co(NO<sub>3</sub>)<sub>2</sub>·6H<sub>2</sub>O ( $\geq 99\%$ , Aldrich), starting powders. The presence of Bi affects the pH of coprecipitation processes compared to previous works [15], being 6.7 for ammonium carbonate, and 8.8 for oxalic acid. After precipitation, they were filtered, washed three times, and dried at 150°C. The mixtures of Bi basic carbonate and Co(II) and Ca carbonates obtained with ammonium carbonate, and the Bi, Ca, and Co oxalates obtained with oxalic acid, were

heated at 450°C to decompose them, producing CaCO<sub>3</sub>, and Co and Bi oxides with small particle sizes (around 50nm).

In attrition milling and solid state, Bi<sub>2</sub>O<sub>3</sub> (99.9%, Aldrich), CaCO<sub>3</sub> (≥99%, Aldrich), and Co<sub>3</sub>O<sub>4</sub> (99.5%, Panreac) have been used as starting powders. They were mixed and milled in an attrition mill at 400rpm using ZrO<sub>2</sub> balls, and in an agate ball mill at 400rpm, respectively, in water for 2h. The slurries were dried obtaining a mixture of CaCO<sub>3</sub>, and Co and Bi oxides with different grain sizes (200nm, and 1μm, respectively).

After these processes, all precursors were thermally treated at 750 and 800°C for 12h, with an intermediate milling, to decompose the CaCO<sub>3</sub>, uniaxially pressed at 400MPa, and sintered at 800°C 24h with final furnace cooling.

Hereafter, samples produced by ammonium carbonate coprecipitation will be named P1, by oxalic acid, P2, the ones by attrition milling, P3, and the solid state ones, P4.

Microstructural observations were performed on the surfaces using a FESEM (Zeiss Merlin) fitted with an EDS system.  $\rho$  and S were determined in a LSR-3 (Linseis GmbH) between 50 and 650°C. Thermal conductivity has been determined using the infrared photothermal radiometry (PTR) which measures thermal diffusivity ( $\alpha$ ) and effusivity ( $e$ ), obtaining  $\kappa$  from  $\kappa = e \sqrt{\alpha}$  [16,17]. At higher temperatures, a Linkam LTS 350 heating stage with an infrared transparent window (CaF<sub>2</sub>) has been used. ZT has been calculated from room temperature (RT) to 200°C, and estimated at higher temperatures considering that  $\kappa$  is maintained unchanged, considering previous results [11].

### 3. Results and discussion

Micrographs of surfaces are displayed in Fig. 1, showing that P1, P2, and P3 samples possess lower porosity and secondary phases content than P4 ones, indicating that P1, P2 and P3 precursors possess high reactivity and homogeneity, due to their smaller particle sizes. Moreover, all samples are composed of three phases (distinguished by their contrasts): Bi<sub>2</sub>Ca<sub>2</sub>Co<sub>1.7</sub>O<sub>x</sub> (grey, #1 in Fig. 1a) as major one, Co-free (white, #2 in Figs. 1a and b), and Bi-free (dark grey, #3 in Figs. 1a and b).

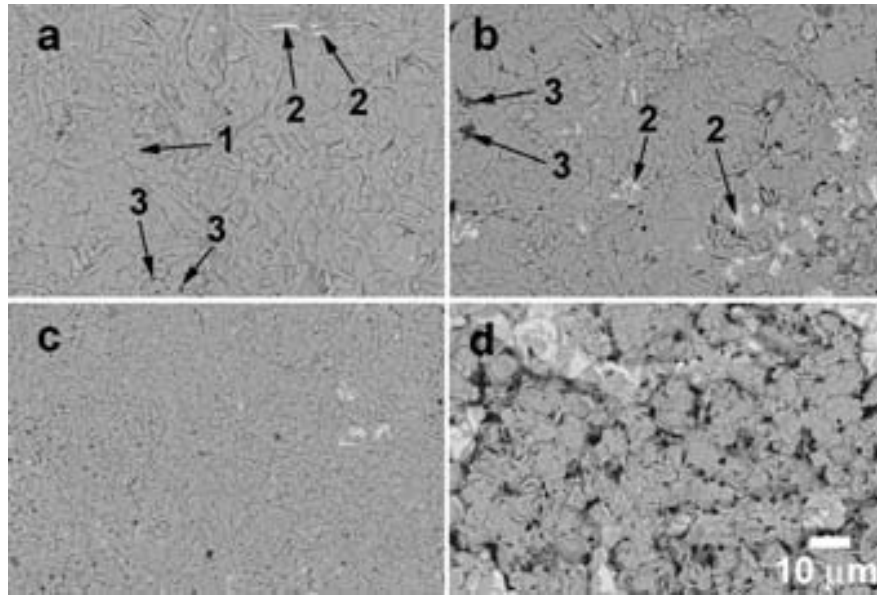


**Fig. 1.** FESEM micrographs obtained in materials prepared from precursors P1 (a), P2 (b), P3 (c), and P4 (d). Numbers indicate different phases: 1)  $\text{Bi}_2\text{Ca}_2\text{Co}_{1.7}\text{O}_x$ ; 2) Bi-Ca-O; and 3) Ca-Co-O.

$\rho$  data, displayed in Fig. 2, agree with these observations. P4 shows semiconducting-like behaviour ( $d\rho/dT < 0$ ) from RT to 550°C and metallic-like one ( $d\rho/dT > 0$ ) at higher temperatures, while the other samples show metallic-like behaviour and lower values in the whole measured temperature range. The minimum values at RT (30m $\Omega$ .cm), are lower than in laser floating zone (LFZ) grown materials (95-120m $\Omega$ .cm) [18], but higher than in single crystals (6m $\Omega$ .cm) [11].

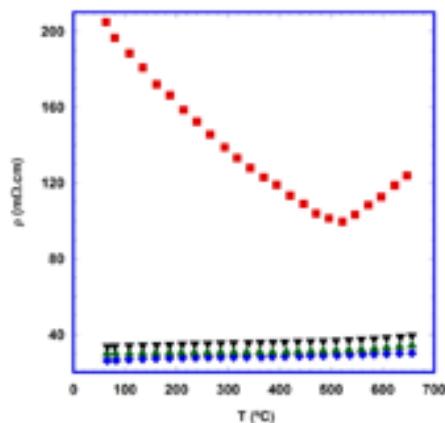


**Fig. 2.** Electrical resistivity vs. temperature of sintered materials prepared from precursors ( $\blacktriangle$ ) P1, ( $\blacktriangledown$ ) P2, ( $\blacklozenge$ ) P3, and ( $\blacksquare$ ) P4.

Fig. 3 displays the S variation with temperature. All samples exhibit positive values in the whole measured temperature range, confirming hole conduction mechanism. P4 samples exhibit

comparable values to those reported elsewhere ( $150\mu\text{V/K}$ ) at RT [19], while they are smaller than the obtained in P1, P2, and P3 ( $170\mu\text{V/K}$ ), comparable to LFZ grown materials ( $170\mu\text{V/K}$ ) [18]. These values are very high for sintered materials, as it is known that LFZ grown materials possess high amount of oxygen vacancies and, consequently, high S values [20]. When comparing with the data for single crystals at RT and  $525^\circ\text{C}$  ( $125$  and  $180\mu\text{V/K}$ , respectively) [11], P1, P2, and P3 samples show much higher values ( $170$  and  $270\mu\text{V/K}$ , respectively).

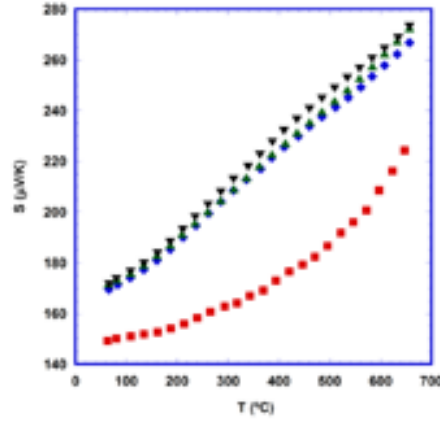


**Fig. 3.** Seebeck coefficient vs. temperature of sintered materials prepared from precursors ( $\blacktriangle$ ) P1, ( $\blacktriangledown$ ) P2, ( $\blacklozenge$ ) P3, and ( $\blacksquare$ ) P4.

The  $\kappa$  values are constant between RT to  $200^\circ\text{C}$ , being  $2.10$ ,  $2.00$ ,  $2.20$ , and  $1.60\text{W/K.m}$  for P1, P2, P3, and P4 samples, respectively. These values agree with microstructural observations and are consistent with reported data in single crystals at high temperature [11]. Moreover, despite the few reports on  $\kappa$  for this material, there are some discrepancies, showing  $\kappa$  values, at  $300\text{K}$ , ranging from  $3$  to  $1\text{W/K.m}$  for bulk solid state or sol-gel prepared samples [19,21,22], which are in agreement with the values measured in this work.

With these data, ZT values have been calculated from RT to  $200^\circ\text{C}$  and estimated at  $650^\circ\text{C}$ , and displayed in Table 1.

**Table 1.** Calculated (at RT and  $200^\circ\text{C}$ ) and estimated (at  $650^\circ\text{C}$ ) ZT values for all samples.

Sample	ZT		
	RT	$200^\circ\text{C}$	$650^\circ\text{C}$
P1	0.016	0.027	0.094
P2	0.015	0.026	0.090
P3	0.017	0.029	0.099
P4	0.002	0.005	0.023

It is clear that using small particle size precursors allows improving ZT (around four times), compared with samples prepared through classical solid state. Even if ZT values are small for practical applications, the maximum values at RT (0.017) are about two times higher than the obtained in sintered materials prepared via solid state or sol-gel (0.008) [21,22]. On the other hand, the calculated ( $\sim 0.017$  at RT) and estimated ( $\sim 0.10$  at  $650^\circ\text{C}$ ) ZT in P1, P2, and P3 materials are still far from the values in single crystals measured along the ab plane (0.13 and 0.25 at RT and  $525^\circ\text{C}$ , respectively). It is worth to mention that the materials prepared in this work are not textured, possess a high number of grain boundaries and some porosity, which raises electrical resistivity and lowers TE performances compared with single crystals.

#### 4. Conclusions

This work demonstrates that nanosized precursors lead to high performances  $\text{Bi}_2\text{Ca}_2\text{Co}_{1.7}\text{O}_x$  thermoelectric materials. They decrease porosity and raise thermoelectric phase content, compared with the solid state route. This is reflected in the simultaneous raise of S, and  $\rho$ . In spite of the  $\kappa$  increase, ZT values are higher than the reported in the literature for bulk sintered materials.

#### Acknowledgements

The authors thank Gobierno de Aragón-Fondo Social Europeo (Grupos de Investigación Consolidados T12 and T87) and MINECO-FEDER (MAT2013-46505-C3-1-R) for financial support. Authors acknowledge the use of Servicio General de Apoyo a la Investigación-SAI, Universidad de Zaragoza. This work was also supported by “le Syndicat Mixte de la Côte d’Opale” and “la région Nord Pas de Calais”.

#### References

1. Rowe DM. In: Rowe DM, editor. Thermoelectrics handbook: macro to nano. 1st ed. Boca Raton, FL: CRC Press; 2006. p. 1-3–1-7.
2. I. Terasaki, Y. Sasago, K. Uchinokura, Phys. Rev. B 56 (1997) 12685-12687.
3. J. C. Diez, E. Guilmeau, M. A. Madre, S. Marinel, S. Lemonnier A. Sotelo, Solid State Ionics 180 (2009) 827-830.

4. K. Rubesova, T. Hlasek, V. Jakes, D. Sedmidubsky, J. Hejtmanek, IOP Conf. Ser.-Mater. Sci. Eng. 30 (2012) 012004.
6. A. Sotelo, Sh. Rasekh, M. A. Madre, E. Guilmeau, S. Marinel, J. C. Diez, J. Eur. Ceram. Soc. 31 (2011) 1763-1769.
6. K. Rubesova, T. Hlasek, V. Jakes, S. Huber, J. Hejtmanek, D. Sedmidubsky, J. Eur. Ceram. Soc. 35 (2015) 525-531.
7. K. Koumoto, I. Terasaki, R. Funahashi, MRS Bull. 31 (2006) 206-210.
8. H. Wang, X. Sun, X. Yan, D. Huo, X. Li, J.-G. Li, X. Ding, J. Alloys Compds. 582 (2014) 294-298.
9. S. Butt, J.-L. Liu, K. Shehzad, B. Zhan, Y. Lin, C.-W. Nan, J. Alloys Compds. 588 (2014) 277-283.
10. N. M. Ferreira, Sh. Rasekh, F. M. Costa, M. A. Madre, A. Sotelo, J. C. Diez, M. A. Torres, Mater. Lett. 83 (2012) 144-147.
11. N. Sun, S. T. Dong, B. B. Zhang, Y. B. Chen, J. Zhou, S. T. Zhang, Z. B. Gu, S. H. Yao, Y. F. Chen, J. Appl. Phys. 114 (2013) 043705.
12. G. Constantinescu, Sh. Rasekh, M. A. Torres, J. C. Diez, M. A. Madre, A. Sotelo, J. Alloys Compds. 577 (2013) 511-515.
13. A. Sotelo, G. Constantinescu, Sh. Rasekh, M. A. Torres, J. C. Diez, M. A. Madre, J. Eur. Ceram. Soc. 32 (2012) 2415-2422.
14. N. Y. Wu, T. C. Holgate, N. V. Nong, N. Pryds, S. Linderoth, J. Eur. Ceram. Soc. 34 (2014) 925-931.
15. A. Sotelo, Sh. Rasekh, M. A. Torres, P. Bosque, M. A. Madre, J. C. Diez, J. Solid State Chem. 221 (2015) 247-254.
16. M. Depriester, P. Hus, S. Delenclos, A. Hadj Sahraoui, Rev. Sci. Instrum. 76 (2005) 074902.
17. D. P. Almond, P. Patel, Photothermal, Science and Techniques, first ed., Chapman & Hall, London (1996).
18. Sh. Rasekh, M. A. Madre, A. Sotelo, E. Guilmeau, S. Marinel, J. C. Diez, Bol. Soc. Esp. Ceram. V. 49 (2010) 89-94.
19. A. Maignan, S. Hebert, M. Hervieu, C. Michel, D. Pelloquin, D. Khomskii, J. Phys.: Condens. Matter. 15 (2003) 2711-2723.
20. J. C. Diez, Sh. Rasekh, M. A. Madre, E. Guilmeau, S. Marinel, A. Sotelo, J. Electron. Mater. 39 (2010) 1601-1605.

21. K. Rubesova, T. Hlasek, V. Jakes, D. Sedmidubsky, J. Hejtmanek, J. Sol-Gel Sci. Technol. 64 (2012) 93-99.
22. L. H. Yin, R. Ang, L. J. Li, B. C. Zhao, Y. K. Fu, X. B. Zhu, Z. R. Yang, W. H. Song, Y. P. Sun, Phys. B 406 (2011) 2914-2918.